JOURNAL OF AIRCRAFT
Vol. 35, No. 5, September–October 1998

Further Refinement of the Subsonic Doublet-Lattice Method

William P. Rodden*
William P. Rodden, Ph.D., Inc., La Cañada Flintridge, California 91011-2838
Paul F. Taylor†
Gulfstream Aerospace Corporation, Savannah, Georgia 31402
and
Samuel C. McIntosh Jr.‡
McIntosh Structural Dynamics, Mountain View, California 94040

The doublet-lattice method (DLM) is in use worldwide for flutter and dynamic response analyses of aircraft at subsonic speeds. The present paper develops a further refinement to extend its frequency limits for applications to higher frequency flutter, e.g., for aeroservoelastic systems with high-frequency control surfaces, and dynamic response, e.g., for short wavelength gusts. The DLM is an aerodynamic finite element method for modeling oscillating interfering lifting surfaces in subsonic flows. It reduces to the vortex-lattice method at zero-reduced frequency. The number of finite elements (boxes) required for accurate results depends on aspect ratio and reduced frequency, among other parameters. At high reduced frequency, the chordwise dimension of the boxes must be small. However, an approximation in the method, viz., that the variation of the numerator of the incremental oscillatory kernel function is parabolic across the span of the box bound vortex, restricts the box aspect ratio to about 3. Hence, high-frequency requirements bring an associated requirement for a large number of boxes in the aerodynamic idealization. If a higher-order approximation is used for the spanwise variation of the numerator of the incremental oscillatory kernel, the limitation on box aspect ratio can be relaxed and the number of spanwise divisions required in high-frequency analyses will be reduced significantly, leading to a reduction in the total number of boxes. This paper replaces the original parabolic approximation by a quartic approximation. The quartic curve-fitting coefficients are determined for the planar and nonplanar kernels, and the new integrals for the planar and nonplanar normalwash factors are evaluated. The refinement is incorporated into a DLM code previously known as N5KA, and convergence studies on typical configurations are presented that attempt to specify a higher limit for practical box aspect ratios.

Nomenclature

A, B, C, D, E = coefficients in quartic approximations to kernel numerators
b_r = reference semichord
C_L = total lift coefficient
D_{rs} = normalwash factor
D_{0rs} = steady normalwash factor
D_{1rs}, D_{2rs} = incremental oscillatory planar and nonplanar normalwash factors, respectively
e = box semiwidth
F = integral in Eq. (21)
K = kernel function
K_1, K_2 = factors in numerators of planar and nonplanar parts of kernel, respectively
k_r = reference reduced frequency, $\omega b_r/U$
M = Mach number
N = number of lifting surfaces
p = lifting pressure coefficient
$Q(\bar{\eta})$ = quartic approximation to kernel numerator
Q_1, Q_2 = approximations for planar and nonplanar numerators, respectively
r = cylindrical radius from sending doublet
S_n = area of nth lifting surface
s = semispan
T = direction cosine function
$T_1, T_{\frac{1}{2}}^*$ = functions for planar and nonplanar parts of kernel, respectively
U = freestream velocity
w = dimensionless normalwash
$\bar{x}$ = streamwise distance between an arbitrary point on the sending line and receiving point
x_0, y_0, z_0 = Cartesian coordinates of receiving point relative to midpoint of sending line (bound vortex)
$\bar{y}, \bar{z}$ = coordinates of receiving point relative to midpoint of sending line parallel and perpendicular to sending box, respectively
γ = dihedral angle
γ_r, γ_s = dihedral angles of receiving and sending boxes, respectively
$\bar{\gamma}_r$ = relative dihedral angle between receiving and sending boxes, $\gamma_r - \gamma_s$
Δx_s = centerline chord of sending box
ε = parameter defined in Eq. (24)
$\bar{\eta}$ = spanwise coordinate, in an element plane
Λ_s = sweepback angle of sending box one-quarter-chord line
ω = circular frequency

Subscripts
1, 2 = planar and nonplanar parts of kernel, respectively

Presented as Paper ICAS-96-2.8.2 at the 20th Congress of the International Council of the Aeronautical Sciences, Sorrento, Italy, Sept. 8–13, 1996; received Oct. 6, 1996; revision received April 6, 1998; accepted for publication April 24, 1998.

*Consulting Engineer.
†Loads and Dynamics Engineer. Senior Member AIAA.
‡Consulting Engineer. Associate Fellow AIAA.

Introduction

THE doublet-lattice method (DLM)[1] is a finite element method for the solution of the oscillatory subsonic pressure–normalwash integral equation for multiple interfering surfaces

$$w(x, s) = \frac{1}{8\pi} \sum_{n=1}^{N} \iint_{S_n} K(x, \xi; s, \sigma) p(\xi, \sigma)\, d\xi\, d\sigma \qquad (1)$$

where (x, s) are the orthogonal coordinates on the nth surface S_n such that the undisturbed stream is parallel to the x axis, and K is the complex acceleration potential kernel for oscillatory subsonic flow. The original DLM algorithm was presented at the same time as the lifting line element method (LLEM) of Landahl and Stark.[2] Although numerous comparisons[2,3] with experiments were shown at the time, the complete details of the LLEM were never published. Stark has written a note on the LLEM, and this was included in Ref. 4 as Appendix A.

A refinement to the expressions for the kernel given by Rodemich in Ref. 5, and Landahl[6] was presented by Rodden et al.[7] in the form

$$K = (K_1 T_1 / r^2 + K_2 T_2^* / r^4) \exp(-i\omega \bar{x}/U) \qquad (2)$$

to analyze nonplanar interference correctly. K_1 and K_2 are the planar and nonplanar parts of the kernel numerator, respectively,

$$T_1 = \cos(\gamma_r - \gamma_s) \qquad (3)$$

$$T_2^* = (z_0 \cos\gamma_r - y_0 \sin\gamma_r)(z_0 \cos\gamma_s - y_0 \sin\gamma_s) \qquad (4)$$

$$r^2 = z_0^2 + y_0^2 \qquad (5)$$

The coordinate system is illustrated in Fig. 1. The description of K_1 and K_2 as the planar and nonplanar parts of the kernel numerator is a convenience because both are obviously nonplanar in general. The refinement in Eq. (2) is in the second term; this was found to be necessary so that the DLM could predict the interference between a *nearly planar* wing and horizontal tail.[7] The refinement retained the original primary approximation,[1] i.e., that the *incremental* oscillatory normalwash factors are obtained by integrating the difference between the oscillatory and steady kernels over the length of the bound vortex assuming a quadratic (parabolic) variation in the numerator of the difference. The total normalwash factor is then the sum of the incremental oscillatory normalwash factor and

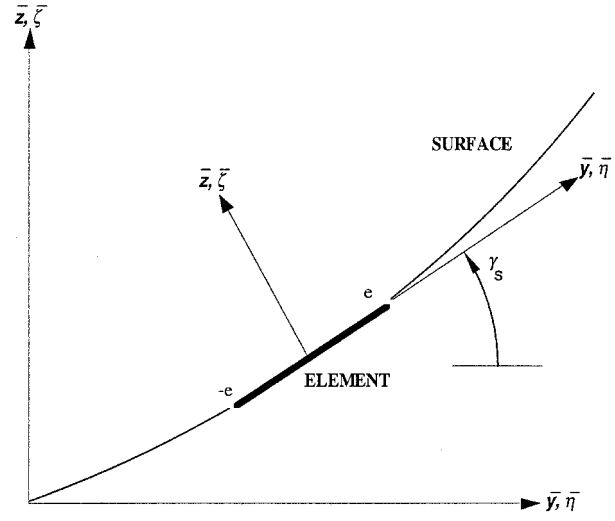

Fig. 1 Lifting surface coordinate system.

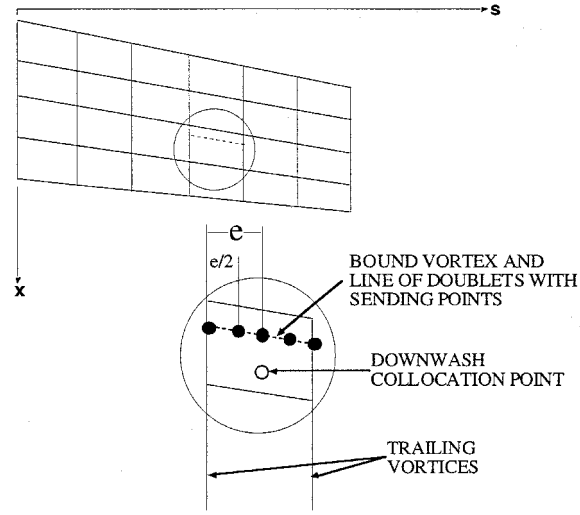

Fig. 2 Idealization of lifting surface using trapezoidal boxes.

the steady normalwash factor obtained from the expressions for a horseshoe vortex, e.g., the vortex-lattice method (VLM) of Hedman.[8] In this way, the DLM converges to the VLM at zero reduced frequency, and the error in the parabolic approximation of the kernel numerator difference is small at low reduced frequencies but increases with reduced frequency.

Extensive experience with the VLM and DLM has led to guidelines for the idealization of lifting surfaces into finite element models. It is assumed that each surface can be approximated by segments of planes. The surface is divided into small trapezoidal panels (boxes) in a manner such that the boxes are arranged in strips parallel to the freestream (Fig. 2) and surface edges and fold lines lie on box boundaries. Boxes should be concentrated near wing edges and hinge lines or any other place where downwash is discontinuous and pressures have large gradients. (The usual practice is not to concentrate boxes near hinge lines because viscous effects, which dominate trailing-edge control-surface aerodynamics, reduce hinge moments from potential theory results, so that more chordwise boxes tend to overpredict hinge moments.) The chord lengths of adjacent boxes in the streamwise direction should only change gradually. If a surface lies in (or nearly in) the plane of another surface, the spanwise divisions of the downstream surface should lie along the spanwise divisions of the upstream surface. Strips at the intersection of lifting surfaces should have approximately equal widths.

The foregoing qualitative modeling recommendations have been quantified (the guidelines have been summarized by Rodden and Johnson[9]) as follows. The aspect ratio of the boxes should be less than three. The chord length of the boxes should be less than 0.08 times the minimum velocity divided by the maximum frequency (in Hz) of interest, i.e., $\Delta x < 0.08U/f$ (this is a requirement for approximately 12 boxes per minimum wave length; however, no less than four boxes per chord should be used). The limitation of box aspect ratio to three is a consequence of the DLM assumption of a parabolic variation in the incremental kernel numerator. The variation of the real part of the incremental kernel numerator along the box quarter-chord is shown in Fig. 3 for an aspect ratio of 2.

Aeroservoelastic analyses frequently deal with high frequencies in control-system components, and new design criteria for short wavelength gusts, e.g., the tuned discrete gust requires a minimum gradient distance of 30 ft be analyzed,[10,11] also require that higher reduced frequencies be considered. The combination of the box chord length limitation and the box aspect ratio limitation can result in a requirement for a large number of aerodynamic boxes. A higher-order (higher than quadratic) approximation to the numerator of the incremental oscillatory kernel will increase the limit on box aspect ratio for accurate

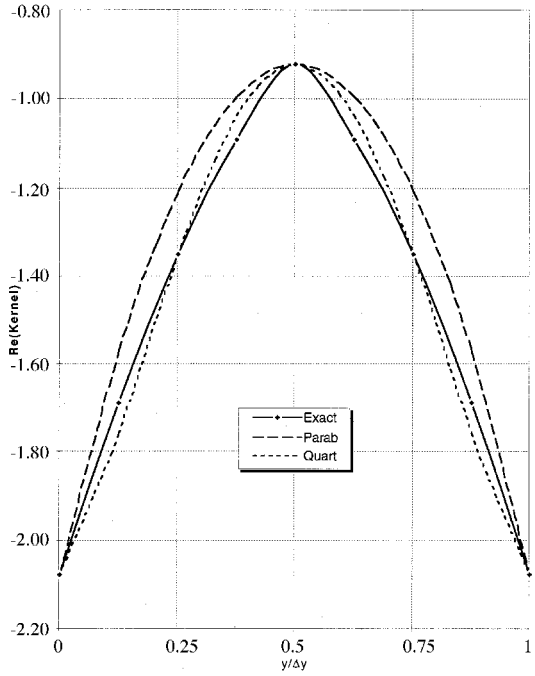

Fig. 3 Variation of incremental kernel along box quarter-chord, aspect ratio = 2.0.

oscillatory aerodynamic analysis. This paper considers a further refinement to the DLM in a quartic approximation and then attempts to determine a new practical limit on maximum box aspect ratio.

New Refinement

The original method for determining the influence of an oscillating lifting surface element at a point was based on the assumption that the lifting pressure could be concentrated along a line. The line is located at the one-quarter-chord line of the element (Fig. 2). The lifting load line is represented by a horseshoe vortex for its steady effects and a line of doublets for its incremental oscillatory effects. The surface boundary condition is a prescribed normalwash at the control point of each box that is located at the three-quarter-chord point along the centerline of each box. The numerical form of the integral equation, Eq. (1), in matrix notation becomes

$$\{w\} = [D]\{p\} \tag{6}$$

where the elements of the normalwash factor matrix $[D]$ are

$$D_{rs} = \frac{\Delta x_s}{8\pi} \int_{-e}^{+e} K \, \mathrm{d}\bar{\eta} \tag{7}$$

Here the streamwise integration of the kernel has been performed by concentrating the lifting pressure at the one-quarter-chord load line.

The evaluation of the normalwash factor, Eq. (7), in element coordinates gives

$$D_{rs} = \frac{\Delta x_s}{8\pi} \int_{-e}^{+e} \left(\frac{K_1 T_1}{r^2} + \frac{K_2 T_2^*}{r^4} \right) \exp\left[-i\omega \frac{(x_0 - \bar{\eta} \tan \lambda_s)}{U} \right] \mathrm{d}\bar{\eta} \tag{8}$$

where $r^2 = (\bar{y} - \bar{\eta})^2 + \bar{z}^2$ and λ_s is the sweep of the one-quarter-chord line of the sending box. The normalwash factor is evaluated as before by adding and subtracting the steady values of K_1 and K_2, denoted by K_{10} and K_{20}, respectively, from their oscillatory counterparts. Then, Eq. (8) becomes

$$D_{rs} = D_{0rs} + D_{1rs} + D_{2rs} \tag{9}$$

where

$$D_{0rs} = \frac{\Delta x_s}{8\pi} \int_{-e}^{+e} \left(\frac{K_{10} T_1}{r^2} + \frac{K_{20} T_2^*}{r^4} \right) \mathrm{d}\bar{\eta} \tag{10}$$

$$D_{1rs} = \frac{\Delta x_s}{8\pi} \int_{-e}^{+e} \frac{\left\{ K_1 \exp\left[-i\omega \frac{(x_0 - \bar{\eta} \tan \lambda_s)}{U} \right] - K_{10} \right\} T_1}{r^2} \mathrm{d}\bar{\eta} \tag{11}$$

$$D_{2rs} = \frac{\Delta x_s}{8\pi} \int_{-e}^{+e} \frac{\left\{ K_2 \exp\left[-i\omega \frac{(x_0 - \bar{\eta} \tan \lambda_s)}{U} \right] - K_{20} \right\} T_2^*}{r^4} \mathrm{d}\bar{\eta} \tag{12}$$

Equation (10) is the steady normalwash factor and is more conveniently derived from horseshoe vortex considerations than by evaluating the integral. The steady normalwash factor has been given by Hedman.[8] We may evaluate the incremental oscillatory normalwash factors [Eqs. (11) and (12)] in closed form by approximating the numerators as quartics in $\bar{\eta}$. We rewrite Eq. (11) as

$$D_{1rs} = \frac{\Delta x_s}{8\pi} \int_{-e}^{+e} \frac{Q_1(\bar{\eta})}{(\bar{y} - \bar{\eta})^2 + \bar{z}^2} \mathrm{d}\bar{\eta} \tag{13}$$

where $Q_1(\bar{\eta})$ is the quartic approximation

$$Q_1(\bar{\eta}) = A_1\bar{\eta}^2 + B_1\bar{\eta} + C_1 + D_1\bar{\eta}^3 + E_1\bar{\eta}^4 \approx \{K_1 \exp[-i\omega(x_0 - \bar{\eta} \tan \lambda_s)/U] - K_{10}\} T_1 \tag{14}$$

If we denote the inboard, inboard intermediate, center, outboard intermediate, and outboard values of $Q_1(\bar{\eta})$, respectively, by $Q_1(-e)$, $Q_1(-e/2)$, $Q_1(0)$, $Q_1(e/2)$, and $Q_1(e)$, the quartic coefficients are

$$A_1 = -(1/6e^2)[Q_1(-e) - 16Q_1(-e/2) + 30Q_1(0) - 16Q_1(e/2) + Q_1(e)] \tag{15}$$

$$B_1 = (1/6e)[Q_1(-e) - 8Q_1(-e/2) + 8Q_1(e/2) - Q_1(e)] \tag{16}$$

$$C_1 = Q_1(0) \tag{17}$$

$$D_1 = -(2/3e^3)[Q_1(-e) - 2Q_1(-e/2) + 2Q_1(e/2) - Q_1(e)] \tag{18}$$

$$E_1 = (2/3e^4)[Q_1(-e) - 4Q_1(-e/2) + 6Q_1(0) - 4Q_1(e/2) + Q_1(e)] \tag{19}$$

Then the planar downwash factor becomes

$$D_{1rs} = \frac{\Delta x_s}{8\pi} \left\{ [(\bar{y}^2 - \bar{z}^2)A_1 + \bar{y}B_1 + C_1 + \bar{y}(\bar{y}^2 - 3\bar{z}^2)D_1 + (\bar{y}^4 - 6\bar{y}^2\bar{z}^2 + \bar{z}^4)E_1]F + \left[\bar{y}A_1 + \frac{1}{2}B_1 + \frac{1}{2}(3\bar{y}^2 - \bar{z}^2)D_1 + 2\bar{y}(\bar{y}^2 - \bar{z}^2)E_1 \right] \log \frac{(\bar{y} - e)^2 + \bar{z}^2}{(\bar{y} + e)^2 + \bar{z}^2} + 2e\left[A_1 + 2\bar{y}D_1 + \left(3\bar{y}^2 - \bar{z}^2 + \frac{1}{3}e^2 \right) E_1 \right] \right\} \tag{20}$$

where the integral

$$F = \int_{-e}^{+e} \frac{\mathrm{d}\bar{\eta}}{(\bar{y} - \bar{\eta})^2 + \bar{z}^2} = \frac{1}{|\bar{z}|} \operatorname{atan}\left(\frac{2e|\bar{z}|}{\bar{y}^2 + \bar{z}^2 - e^2} \right) \tag{21}$$

is evaluated as before.[7] The integral F may be rewritten as

$$F = \delta_1 \frac{2e}{\bar{y}^2 + \bar{z}^2 - e^2}\left(1 - \varepsilon\frac{\bar{z}^2}{e^2}\right) + \delta_2\frac{\pi}{|\bar{z}|} \tag{22}$$

where

$$\begin{aligned}
&\delta_1 = 1,\ \delta_2 = 0 \quad \text{for} \quad \bar{y}^2 + \bar{z}^2 - e^2 > 0\\
&\delta_1 = 1,\ \delta_2 = \frac{1}{2} \quad \text{for} \quad \bar{y}^2 + \bar{z}^2 - e^2 = 0\\
&\delta_1 = 1,\ \delta_2 = 1 \quad \text{for} \quad \bar{y}^2 + \bar{z}^2 - e^2 < 0
\end{aligned} \tag{23}$$

to place the arctangent in the correct quadrant, and

$$\varepsilon = \frac{e^2}{\bar{z}^2}\left[1 - \frac{\bar{y}^2 + \bar{z}^2 - e^2}{2e|\bar{z}|}\operatorname{atan}\left(\frac{2e|\bar{z}|}{\bar{y}^2 + \bar{z}^2 - e^2}\right)\right] \tag{24}$$

When $|2e\bar{z}/(\bar{y}^2 + \bar{z}^2 - e^2)| \le 0.3$, the following series expansion is used

$$\varepsilon = \frac{4e^4}{(\bar{y}^2 + \bar{z}^2 - e^2)^2}\sum_{n=2}^{7}\frac{(-1)^n}{2n-1}\left(\frac{2e|\bar{z}|}{\bar{y}^2 + \bar{z}^2 - e^2}\right)^{2n-4} \tag{25}$$

It is immediately seen that for cases $\bar{y}^2 + \bar{z}^2 - e^2 \le 0$, that F becomes singular like $\pi/|\bar{z}|$ and $\pi/2|\bar{z}|$, respectively. However, it can be shown that a similar contribution (of opposite sign) arises from the nonplanar part that exactly cancels this singular term. Thus, the usual practice for planar cases is to evaluate the Mangler principal part of F, where these two singularities are canceled analytically.[12]

The incremental nonplanar oscillatory normalwash factor is approximated by

$$D_{2rs} = \frac{\Delta x_s}{8\pi}\int_{-e}^{+e}\frac{Q_2(\bar{\eta})}{[(\bar{y} - \bar{\eta})^2 + \bar{z}^2]^2}\,d\bar{\eta} \tag{26}$$

where $Q_2(\bar{\eta})$ is another quartic approximation

$$\begin{aligned}
Q_2(\bar{\eta}) &= A_2\bar{\eta}^2 + B_2\bar{\eta} + C_2 + D_2\bar{\eta}^3 + E_2\bar{\eta}^4\\
&\approx \{K_2\exp[-i\omega(x_0 - \bar{\eta}\tan\lambda_s)/U] - K_{20}\}T_2^*
\end{aligned} \tag{27}$$

Letting $Q_2(-e)$, $Q_2(-e/2)$, $Q_2(0)$, $Q_2(e/2)$, and $Q_2(e)$ denote the inboard, inboard intermediate, center, outboard intermediate, and outboard values of $Q_2(\bar{\eta})$, respectively, we have

$$\begin{aligned}
A_2 = {} & -(1/6e^2)[Q_2(-e) - 16Q_2(-e/2) + 30Q_2(0)\\
& - 16Q_2(e/2) + Q_2(e)]
\end{aligned} \tag{28}$$

$$B_2 = (1/6e)[Q_2(-e) - 8Q_2(-e/2) + 8Q_2(e/2) - Q_2(e)] \tag{29}$$

$$C_2 = Q_2(0) \tag{30}$$

$$D_2 = -(2/3e^3)[Q_2(-e) - 2Q_2(-e/2) + 2Q_2(e/2) - Q_2(e)] \tag{31}$$

$$\begin{aligned}
E_2 = {} & (2/3e^4)[Q_2(-e) - 4Q_2(-e/2) + 6Q_2(0) - 4Q_2(e/2)\\
& + Q_2(e)]
\end{aligned} \tag{32}$$

The nonplanar downwash factor is then given by Eq. (33):

$$\begin{aligned}
D_{2rs} = {} & \frac{\Delta x_s}{16\pi\bar{z}^2}\Bigg(\{(\bar{y}^2 + \bar{z}^2)A_2 + \bar{y}B_2 + C_2 + \bar{y}(\bar{y}^2 + 3\bar{z}^2)D_2\\
& + (\bar{y}^4 + 6\bar{y}^2\bar{z}^2 - 3\bar{z}^4)E_2\}F + \frac{1}{(\bar{y} + e)^2 + \bar{z}^2}\{[(\bar{y}^2 + \bar{z}^2)\bar{y}\\
& + (\bar{y}^2 - \bar{z}^2)e]A_2 + (\bar{y}^2 + \bar{z}^2 + \bar{y}e)B_2 + (\bar{y} + e)C_2\\
& + [\bar{y}^4 - \bar{z}^4 + (\bar{y}^2 - 3\bar{z}^2)\bar{y}e]D_2 + [(\bar{y}^4 - 2\bar{y}^2\bar{z}^2 - 3\bar{z}^4)\bar{y}\\
& + (\bar{y}^4 - 6\bar{y}^2\bar{z}^2 + \bar{z}^4)e]E_2\} - \frac{1}{(\bar{y} - e)^2 + \bar{z}^2}\{[(\bar{y}^2 + \bar{z}^2)\bar{y}\\
& - (\bar{y}^2 - \bar{z}^2)e]A_2 + (\bar{y}^2 + \bar{z}^2 - \bar{y}e)B_2 + (\bar{y} - e)C_2\\
& + [\bar{y}^4 - \bar{z}^4 - (\bar{y}^2 - 3\bar{z}^2)\bar{y}e]D_2 + [(\bar{y}^4 - 2\bar{y}^2\bar{z}^2 - 3\bar{z}^4)\bar{y}\\
& - (\bar{y}^4 - 6\bar{y}^2\bar{z}^2 + \bar{z}^4)e]E_2\} + \left[\bar{z}^2\log\frac{(\bar{y} - e)^2 + \bar{z}^2}{(\bar{y} + e)^2 + \bar{z}^2}\right]D_2\\
& + 4\bar{z}^2\left[e + \bar{y}\log\frac{(\bar{y} - e)^2 + \bar{z}^2}{(\bar{y} + e)^2 + \bar{z}^2}\right]E_2\Bigg)
\end{aligned} \tag{33}$$

$$\begin{aligned}
D_{2rs} = {} & \frac{e\Delta x_s}{8\pi(\bar{y}^2 + \bar{z}^2 - e^2)}\Bigg\{\frac{1}{[(\bar{y} + e)^2 + \bar{z}^2][(\bar{y} - e)^2 + \bar{z}^2]}\\
& \times [2(\bar{y}^2 + \bar{z}^2 + e^2)(e^2A_2 + C_2) + 4\bar{y}e^2B_2 + 2\bar{y}(\bar{y}^4 - 2e^2\bar{y}^2\\
& + 2\bar{y}^2\bar{z}^2 + 3e^4 + 2e^2\bar{z}^2 + \bar{z}^4)D_2 + 2(3\bar{y}^6 - 7e^2\bar{y}^4 + 5\bar{y}^4\bar{z}^2\\
& + 6e^4\bar{y}^2 + 6e^2\bar{y}^2\bar{z}^2 - 3e^2\bar{z}^4 - \bar{z}^6 + \bar{y}^2\bar{z}^4 - 2e^4\bar{z}^2)E_2]\\
& - \frac{(\delta_1\varepsilon + \Delta)}{e^2}[(\bar{y}^2 + \bar{z}^2)A_2 + \bar{y}B_2 + C_2 + \bar{y}(\bar{y}^2 + 3\bar{z}^2)D_2\\
& + (\bar{y}^4 + 6\bar{y}^2\bar{z}^2 - 3\bar{z}^4)E_2]\Bigg\} + \frac{\Delta x_s}{8\pi}\Bigg\{\frac{D_2}{2}\log\frac{(\bar{y} - e)^2 + \bar{z}^2}{(\bar{y} + e)^2 + \bar{z}^2}\\
& + 2\left[e + \bar{y}\log\frac{(\bar{y} - e)^2 + \bar{z}^2}{(\bar{y} + e)^2 + \bar{z}^2}\right]E_2\Bigg\}
\end{aligned} \tag{34}$$

where

$$\Delta = \left(\frac{e}{|\bar{z}|}\right)^2\left[1 - \delta_1 - \delta_2\frac{\pi}{|\bar{z}|}\left(\frac{\bar{y}^2 + \bar{z}^2 - e^2}{2e}\right)\right] \tag{35}$$

The simplification of Eq. (33) via Eq. (22) leading to Eq. (34) is tedious but results in the more accurate form in which ε is again given by Eq. (24). Equation (34) has been used in general, except when $|(\bar{y}^2 + \bar{z}^2 - e^2)/2e\bar{z}| \le 0.1$, in which case Eq. (33) is used.

Two integrals are involved in the evaluation of the kernel function that have utilized approximations to the function $1 - u/\sqrt{(1 + u^2)}$. The original work[1] used an approximation developed by Watkins et al.[13] and later work[14] used a more accurate approximation of Laschka.[15]

An improved approximation developed by Desmarais[16] has the form

$$1 - \frac{u}{\sqrt{(1 + u^2)}} = \sum_{k=1}^{n} a_k\exp[-(2^{k/m})bu] \tag{36}$$

and Desmarais has obtained the coefficients b and a_k corresponding to various values of m and n for n varying from 8 to 72. The 12-term approximation D12.1 has also been used here and its parameters are shown next:

$$\begin{aligned}
a_1 &= 0.000319759140, & a_2 &= -0.000055461471\\
a_3 &= 0.002726074362, & a_4 &= 0.005749551566\\
a_5 &= 0.031455895072, & a_6 &= 0.106031126212\\
a_7 &= 0.406838011567, & a_8 &= 0.798112357155\\
a_9 &= -0.417749229098, & a_{10} &= 0.077480713894\\
a_{11} &= -0.012677284771, & a_{12} &= 0.001787032960
\end{aligned}$$

($n = 12$, $m = 1$, and $b = 0.009054814793$)

Table 1 compares results following Ref. 7 based on the parabolic fitting of the kernels and Laschka's approximation (re-

Table 1 Comparison of lift coefficients, $C_L/ik(h/s)$ for plunging of AGARD wing–tail

Boxes[a]	Parabolic with L11	Parabolic with D12.1	Boxes[b]	Quartic with L11	Quartic with D12.1
108	$3.792+i2.955$	$3.770+i2.965$	72	$3.751+i2.932$	$3.724+i2.935$
132	$3.961+i2.963$	$3.938+i2.974$	88	$3.913+i2.928$	$3.884+i2.932$
168	$4.160+i2.974$	$4.136+i2.986$	112	$4.098+i2.952$	$4.069+i2.957$
216	$4.299+i2.960$	$4.274+i2.973$	144	$4.251+i2.966$	$4.219+i2.972$
264	$4.359+i2.955$	$4.333+i2.969$	176	$4.341+i2.969$	$4.309+i2.975$

[a]Twelve spanwise strips.
[b]Eight spanwise strips.

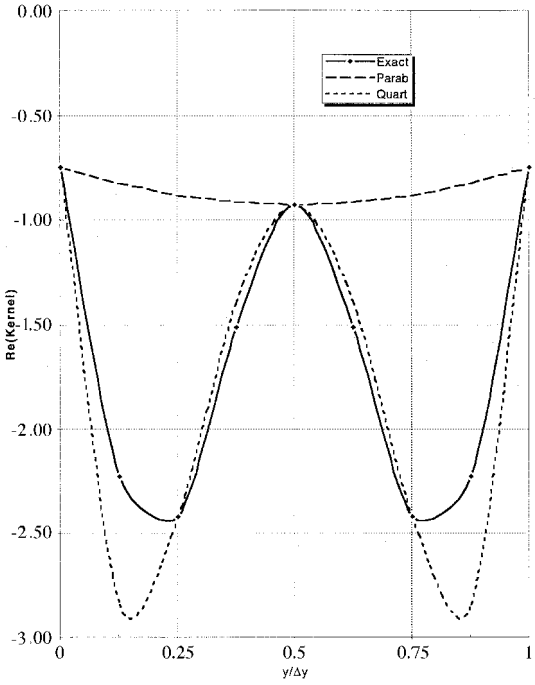

Fig. 4 Variation of incremental kernel along box quarter-chord, aspect ratio = 5.0.

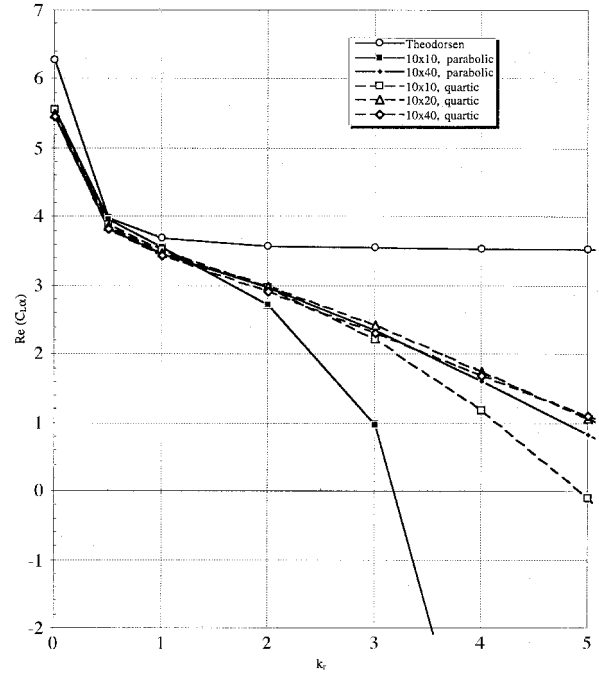

Fig. 5 Re($C_{L\alpha}$) vs k_r, aspect ratio = 20 wing, Mach = 0.0.

ferred to as L11) and Desmarais' approximation (referred to as D12.1), and also the quartic fits with both L11 and D12.1.

Applications

Figures 3 and 4 show the variation of the real part of the incremental kernel numerator along the box quarter-chord for two aspect ratios for a rectangular box with a unit Δx. The receiving point is on the box itself. The Mach number is M = 0.8 and the reduced frequency is k_r = 1.0 based on the box semichord of 0.5. The improved performance of the quartic approximation is evident in the two figures and clearly superior with a box aspect ratio of 5.

Three examples are now considered to illustrate the improved convergence characteristics of the quartic approximation. Each example has been investigated in earlier studies. The first two examples are planar: A high-aspect ratio rectangular wing and a wing–tail combination. The third example is a simplified rectangular T-tail.

High-Aspect Ratio Rectangular Wing

A high-aspect ratio, unswept, untapered rectangular wing can be used conveniently to investigate the requirements for box shapes (aspect ratio) and sizes (number of boxes on a chord). At a Mach number of zero, the calculated loads can also be compared to classical two-dimensional solutions if the aspect ratio is high enough, although it should be noted that there are quantitative differences between pressures at cross sections of a wing with a finite aspect ratio (however large) and a two-dimensional airfoil.

An aspect ratio of 20 is selected, and the symmetric motion of pitching about the midchord is investigated.

Figures 5 and 6 show the real and imaginary parts, respectively, of the lift due to pitch about the midchord. The numbers in the legend, e.g., 10 × 20, refer to the number of chordwise and spanwise boxes, respectively. The results show that the quartic solution with 20 spanwise strips is closer to the converged solution than the parabolic solution with 40 spanwise strips. In fact, the quartic solution with 10 spanwise boxes has acceptable accuracy up to a reduced frequency of 3.

Figures 7 and 8 show the effect of box aspect ratio on convergence for the same wing. Additional cases were calculated with five chordwise boxes. The real part converges more slowly than the imaginary part; however, the quartic is closer to convergence with far fewer boxes than the parabolic approximation. The immediate implications of this are that existing models are accurate to a higher reduced frequency without any change. Conversely, smaller models can be generated to give the same accuracy as the parabolic approximation.

Wing/Horizontal-Stabilizer Combination

This configuration is one of those selected by the AGARD Structures and Materials Panel for comparison of methods used in interfering lifting surface theories. The planar configuration is shown in Fig. 9 with its span divided into 12 strips. The convergence characteristics of the original DLM were studied on this configuration by Rodden et al.[7] with a number of different chordwise box divisions on the wing and tail. The number of boxes with equal chordwise fractions on the wing and

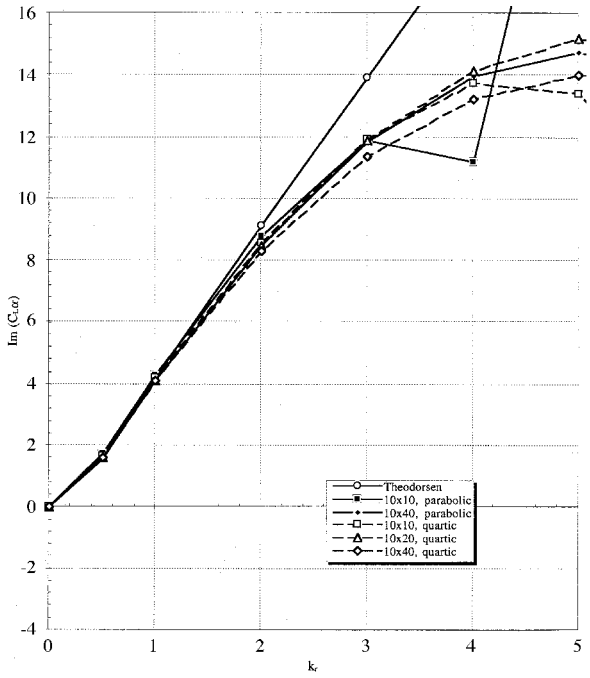

Fig. 6 Im($C_{L\alpha}$) vs k_r, aspect ratio = 20 wing, Mach = 0.0.

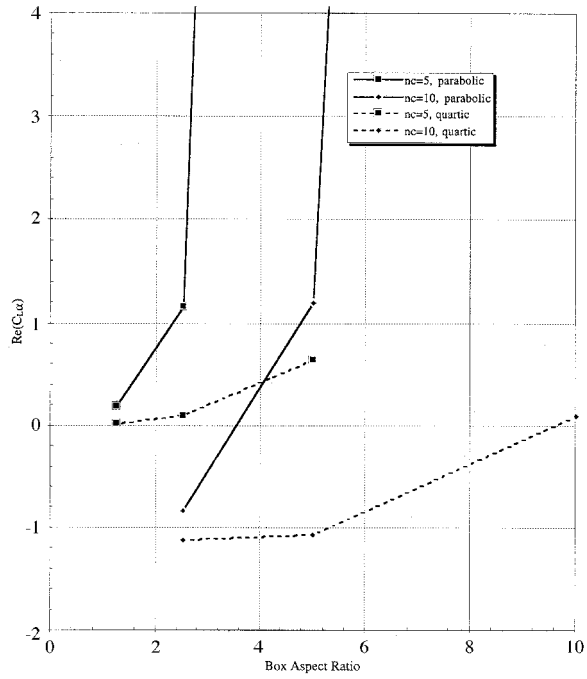

Fig. 7 Effect of box aspect ratio on convergence, aspect ratio = 20 wing, Mach = 0.0, k_r = 5.0.

tail, respectively, were 5 and 4, 6 and 5, 8 and 6, 10 and 8, and 12 and 10.

The 12 spanwise strips were the same for all combinations of boxes, and so the total number of boxes in the various idealizations were 108, 132, 168, 216, and 264. The lift coefficient for oscillatory plunging was obtained at a Mach number of 0.8 and a reduced frequency of $k = \omega s/V = 1.5$, where s is the semispan (based on $b_r = 0.8$, $k_r = 1.2$), and the results are shown in Table 1 with both the Laschka (L11) and Desmarais (D12.1) approximations. (The values labeled "Parabolic" have been recalculated using slightly different strip widths scaled from Fig. 2 of Ref. 7; the actual widths were not reported other than in the figure shown.) The new results with the quartic approximation have been added to Table 1 for an idealization with the same number of chordwise boxes but with only eight spanwise strips (with divisions at 0.0, 0.1667, 0.333, 0.5, 0.6667, 0.8333, 0.9, 0.96, and 1.0 fractions of the span), leading to a total number of boxes of 72, 88, 112, 144, and 176 for the different chordwise divisions. Again, both L11 and D12.1 results are shown. A perusal of Table 1 shows that the quartic approximation with fewer spanwise strips has the same accuracy as the earlier parabolic approximation. The convergence of both sets of results with increasing number of chordwise boxes shows the importance of a sufficient number of chordwise boxes per wavelength: 12 as suggested in the published guidelines.[9] The performance of the quartic approximation in this example suggests an increase in the guideline box aspect ratio limit of 3, established for the parabolic approximation, to perhaps 5 for the quartic approximation.

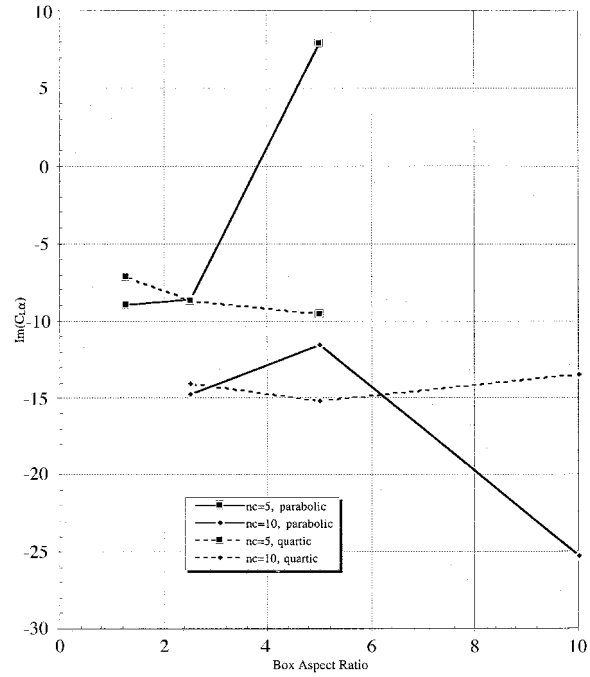

Fig. 8 Effect of box aspect ratio on convergence, aspect ratio = 20 wing, Mach = 0.0, k_r = 5.0.

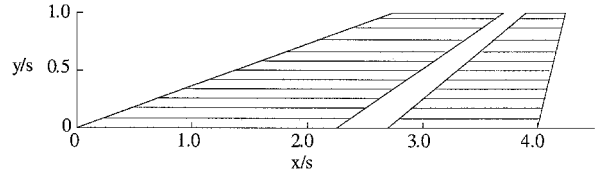

Fig. 9 Wing/horizontal tail configuration.

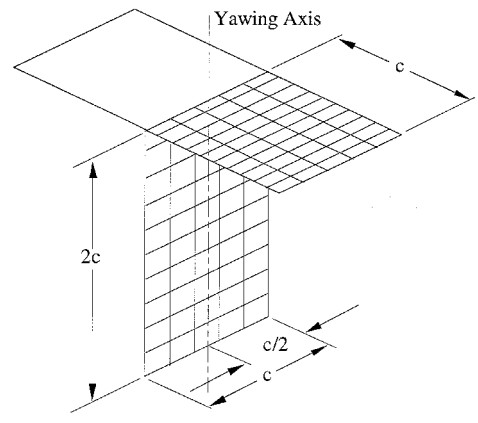

Fig. 10 Rectangular T-tail configuration.

Rectangular T-Tail

The rectangular T-tail that was tested by Clevenson and Leadbetter[17] has also been the subject of previous studies. The wind-tunnel tests were performed at low speed and the model was oscillated about the fin midchord as shown in Fig. 10. The lattice idealization in the earlier study[7] is also shown in the figure. The present study uses equal rectangular boxes chordwise and equal spanwise on the vertical tail and equal boxes chordwise on the horizontal tail. The spanwise variation in fraction of semispan is 0.0, 0.05, 0.17, 0.3, 0.4, 0.5, 0.6, 0.7, 0.8, 0.9, and 1.0, with the spacing at the inboard edge to give comparable strip widths on the vertical and horizontal tail at the intersection. The earlier study[7] and experiment[17] nondimensionalized the coefficients in nonstandard ways. The present study uses a reference semichord of $b_r = c/2 = 0.5$ ft, fin area to normalize the forces and fin span to normalize the moments. Figure 11 shows the variation with reduced frequency of the magnitude and phase angle of the rolling moment (about an axis 0.5 ft below the base of the fin) due to an oscillatory rigid body yawing of the fin about its midchord. The quartic approximation gives the same results as the original study for these low reduced frequencies.[7] Figure 12 shows that a reduction in the number of spanwise strips from 10 to 5 indicates the quartic approximation to have the same accuracy as the earlier study.[7]

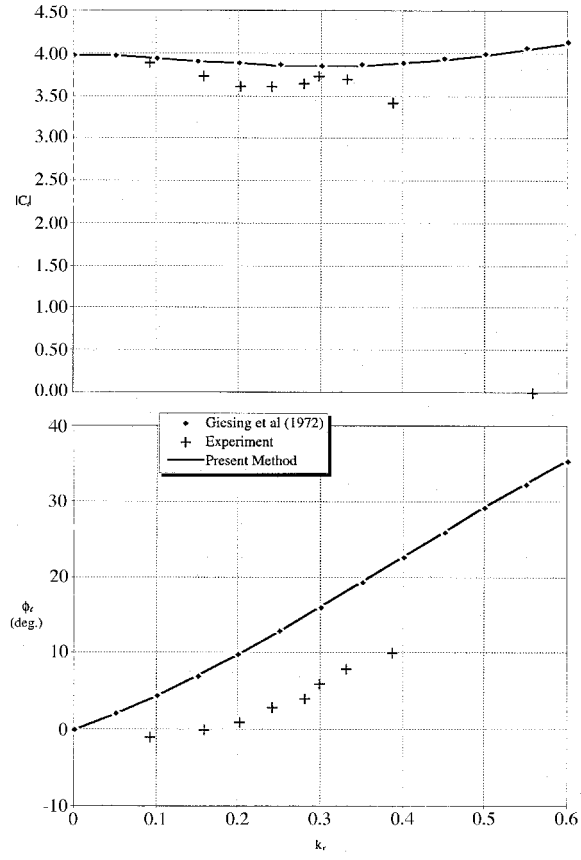

Fig. 11 Rolling moment coefficient vs k_r for T-tail.

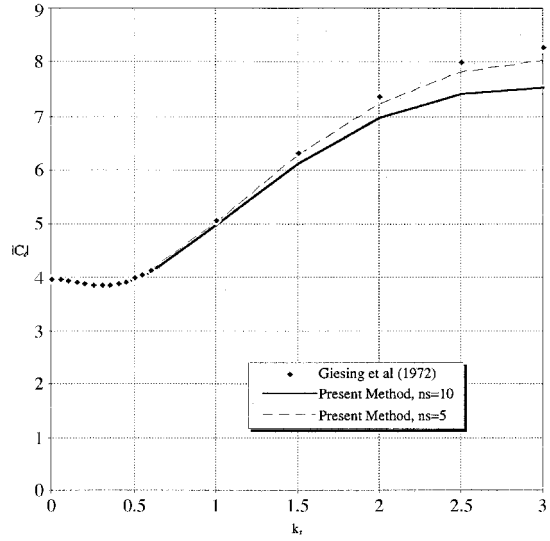

Fig. 12 Effect of number spanwise boxes on C_l, T-tail.

Concluding Remarks

A refinement to the doublet-lattice subsonic lifting surface method has been formulated and implemented. The quartic approximation to the kernel function allows either an increase in accuracy for current box schemes, or a reduction in the number of boxes (and subsequently the storage requirements) for the same accuracy. From the results presented, the limit on box aspect ratio (formerly 3 with the original method) can now be relaxed to 5. This also allows a little more flexibility in modeling because boxes tend to have a higher aspect ratio near the tips of tapered surfaces.

The present study has only considered rigid body modes at a small number of Mach numbers and reduced frequencies. Further analyses are needed to more accurately establish the maximum value of box aspect ratio, tentatively proposed at 5. Another guideline is also needed because a minimum number of spanwise strips has never been established for the previous DLM. This would be a function of the aspect ratio of the lifting surface and its vibration modeshapes, i.e., the number of node lines across the span. Further studies are planned on more practical configurations and the convergence characteristics of the new DLM will be investigated in future flutter and gust response analyses.

A computer program now called N5KQ incorporates the quartic feature of this paper and the Desmarais D12.1 approximation, and is available from the authors, and will be available in a forthcoming release of MSC/NASTRAN.

Acknowledgment

The analytical development was performed while the first author was a Visiting Professor of Aerospace Engineering at the Technion—Israel Institute of Technology, Haifa, Israel, during April–June 1995.

References

[1]Albano, E., and Rodden, W. P., "A Doublet-Lattice Method for Calculating Lift Distributions on Oscillating Surfaces in Subsonic Flows," *AIAA Journal*, Vol. 7, 1969, pp. 279–285; also Erratum, 1969, p. 2192.

[2]Landahl, M. T., and Stark, V. J. E., "Numerical Lifting-Surface Theory–Problems and Progress," *AIAA Journal*, Vol. 6, 1968, pp. 2049–2060.

[3]Wittmeyer, H., "Aeroelastomechanische Untersuchungen an dem Flugzeug SAAB 37'Viggen'," *Ludwig Prandtl-Gedächtnis Vorlesung*, Munich, Germany, Jahrbuch 1968, pp. 11–23.

[4]Rodden, W. P., Taylor, P. F., and McIntosh, S. C., "Further Refinement of the Nonplanar Aspects of the Subsonic Doublet-Lattice Lifting Surface Method," 20th Congress of the International Council of the Aeronautical Sciences, Sorrento, Italy, Sept. 1996 (Paper 96.2.3).

[5]Vivian, H. T., and Andrew, L. V., "Unsteady Aerodynamics for Advanced Configurations: Part I—Application of the Subsonic Kernel Function to Nonplanar Lifting Surfaces," U.S. Air Force Flight Dynamics Lab., Rept. FDL-TDR-64-152, 1965.

[6]Landahl, M. T., "Kernel Function for Nonplanar Oscillating Surfaces in a Subsonic Flow," *AIAA Journal*, Vol. 5, 1967, pp. 1045, 1046.

[7]Rodden, W. P., Giesing, J. P., and Kálmán, T. P., "Refinement of the Nonplanar Aspects of the Subsonic Doublet-Lattice Lifting Surface Method," *Journal of Aircraft*, Vol. 9, No. 1, 1972, pp. 69–73.

[8]Hedman, S. G., "Vortex Lattice Method for Calculation of Quasi

Steady State Loadings on Thin Elastic Wings," Aeronautical Research Inst. of Sweden, Rept. 105, Stockholm, Sweden, 1967.

[9]Rodden, W. P., and Johnson, E. H., *"MSC/NASTRAN Aeroelastic Analysis User's Guide*," The MacNeal-Schwendler Corp., 1994.

[10]Anon., "Federal Aviation Regulations—Part 25—Airworthiness Standards: Transport Category Airplanes," Dept. of Transportation, Federal Aviation Administration, Washington, DC.

[11]Anon., "Joint Airworthiness Requirements—JAR 25, Large Airplanes," Civil Aviation Authority, Cheltenham, England, UK.

[12]Mangler, K. W., "Improper Integrals in Theoretical Aerodynamics," Royal Aircraft Establishment, Rept. Aero 2424, C.P. No. 94, 1951.

[13]Watkins, C. E., Woolston, D. S., and Cunningham, H. J., "A Systematic Kernel Function Program for Determining Aerodynamic Forces on Oscillating or Steady Finite Wings at Subsonic Speeds," NASA R-48, 1959.

[14]Kálmán, T. P., Rodden, W. P., and Giesing, J. P., "Application of the Doublet-Lattice Method to Nonplanar Configurations in Subsonic Flow," *Journal of Aircraft*, Vol. 8, No. 6, 1971, pp. 406–413.

[15]Laschka, B., "Zur Theorie der harmonisch schwingenden tragenden Fläch bei Unterschallanströmung," *Zeitschrift für Flugwissenschaften*, Vol. 11, No. 7, 1963, pp. 265–292.

[16]Desmarais, R. N., "An Accurate Method for Evaluating the Kernel of the Integral Equation Relating Lift to Downwash in Unsteady Potential Flow," AIAA Paper 82-687, April 1982.

[17]Clevenson, S. A., and Leadbetter, S. A., "Measurements of Aerodynamic Forces and Moments at Subsonic Speeds on a Simplified T-Tail Oscillating in Yaw About The Fin Midchord," NACA TN 4402, 1958.